



Biosynthesised Sm₂O₃ NPs as an efficient catalyst for the preparation of morpholine and piperidine derivatives

S. Marziyeh Kazemi¹, Asieh Yahyazadeh^{*1}, Navabeh Nami^{*2}

¹Department of Chemistry, Faculty of Sciences, University of Guilan, PO Box 41335-1914, Rasht, Iran;

²Department of Chemistry, Qaemshahr Branch, Islamic Azad University, Qaemshahr, Iran.

Received: 11 October 2021; Accepted: 12 January 2022

*Corresponding author email: yahyazadehphd@yahoo.com, navabehnami@yahoo.com

ABSTRACT

Biosynthesis of Sm₂O₃ NPs using Sm(NO₃)₃.6H₂O and double bloom purple Rose of Sharon in ethanol, produced an efficient catalyst for the synthesis of some nitrogen-containing heterocycles such as morpholine and piperidine derivatives. Sm₂O₃ nanoparticles have been confirmed by FT-IR, scanning electron microscopy (SEM), transmission electron microscopy (TEM), X-ray diffraction (XRD), and Energy-dispersive X-ray spectroscopy (EDX). The products were obtained in moderate to good yields under mild reaction conditions and identified by CHN analysis, NMR, and FT-IR spectra. The catalyst could be easily separated from the reaction mixture by centrifugation, washed, dried, and re-entered to a fresh reaction mixture 4 times without considerable loss of activity.

Keywords: Morpholine, piperidine, extract, Sm₂O₃ nanoparticles, green synthesis.

1. Introduction

Nitrogen-containing heterocyclic compounds like morpholine or piperidine derivatives are very important chemical compounds, with a wide variety of research dedicated to the development of novel structures. Over the past two decades, they have received increasing attention from scientists because of their biological and pharmacological activities [1-6]. They are very important chemical structures [7, 8] in drug discovery and also good intermediates for the synthesis of some important organic compounds [9-11]. There have been great advances in the development of numerous heterocyclic synthesis protocols and catalytic methods [12,13].

Scientists are very interested in the biosynthesis of nanomaterials because this method focuses on the production of the desired product without producing harmful intermediate byproducts

during the chemical reaction [14,15]. The rare earth oxide nanoparticles (REO NPs) such as samarium, yttrium, europium, and cerium, gained much attention as important metal oxide NPs due to various applications, including sensors, selective electrodes, and catalysis [16–18]. They have gained considerable importance in organic synthesis because of their small size, large specific surface area, ease of handling, enhanced reaction rates, high selectivity, and simple workup [19–21]. They show good catalytic properties in several reactions including synthesis of ammonia and oxidative coupling of methane [22]. Samarium oxide nanoparticle (Sm₂O₃ NPs) is one of the main rare earth oxide nanomaterials owing to their intrinsic properties which is used in various fields such as nano-electronics, optics, infrared radiation-absorbing glass, solar cells, semiconductors, sensors, and catalyst [23-27]. According to the

above reasons, we predict that samarium oxide nanoparticles can be helpful to increase catalytic activity for the synthesis of morpholine or piperidine derivatives. So in connection with our previous studies on the biosynthesis of catalyst, design, and synthesis of heterocyclic compounds [28–30], we present an effective catalyst for design and synthesis of new derivatives of some morpholine and piperidine in ethanol. Hibiscus Syriacus Ardens belongs to the Malvaceae family, known as Rose of Sharon, was used for the synthesis of Sm_2O_3 NPs.

2. Experimental

2.1. Chemicals and Instrumentation

All chemicals and solvents were purchased from Merck and Aldrich. The production of nano compounds was monitored by measuring the UV-Vis spectrophotometer (JENWAY 650), in the wavelength range of A200 to A800 nm and determined by powder X-ray diffraction (XRD) PW 3040/60 X'Pert PRO diffractometer system, using Cu Ka radiation with ($\lambda = 1.5418 \text{ \AA}$) in the range of $2\theta = 20\text{--}80^\circ$ at room temperature. The morphology and sizes of NPs were evaluated using a scanning electron microscope (SEM) and transmission electron microscope (TEM, 150 kV, and Philips-CM 10) by Daypetronic Company-Iran. FT-IR measurements were recorded on a Shimadzu 8400s spectrometer with KBr plates. The NMR spectra were recorded on Bruker XL 400 (400 MHz) instruments; Mass-spectrometric measurements were made on an Agilent 6890 N Network GC system. The C, H, N analyses were performed by the microanalytical service of Daypetronic Company. Melting points were determined on an Electrothermal 9100 without further corrections.

2.2. Preparation of Sm_2O_3 NPs

Purple Rose of Sharon was collected from Mazandaran, a province north of Iran. The flower was first washed thoroughly in DI water, dried at room temperature for one week, and then ground in a blender before extraction.

The powdered Rose of Sharon flower was weighted (500 g) in a beaker and percolated with ethanol. This beaker was properly covered with aluminum foil and left for 72 hours. The solution was then filtered using a funnel filled in a filter paper and the extract was obtained. It was concentrated using a rotary evaporator and stored in the refrigerator at 4°C before use.

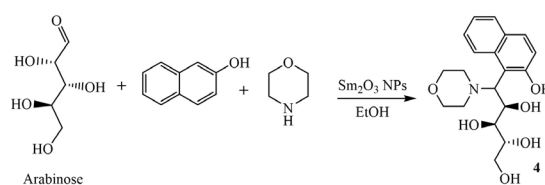
Rose of Sharon flower extract (0.5 g) was dispersed into 50 ml of ethanol: H_2O (1:1). The aqueous solution of $\text{Sm}(\text{NO}_3)_3 \cdot 6\text{H}_2\text{O}$ (0.3 g) in water (20 ml) was added dropwise into the reaction mixture through a dropping funnel by ultrasonication for 30 min and gently stirred at 60°C using a temperature-controlled magnetic stirrer for 2 h, after that 0.02 M NaOH was added dropwise to the solution to achieve the pH 10. The mixture was stirred for 24 extra hours. The completion of the reaction was monitored by UV-Vis spectra at 300-600 nm ($\lambda_{\text{max}} = 244, 324 \text{ nm}$). After completion of the reaction, the precipitate was purified by several re-dispersions in deionized water and then centrifuged at 8000 rpm for 20 min, dried at 100°C . The solid samples were then calcined at 500°C for 4 h.

2.3. General procedure for the synthesis of morpholine and piperidine derivatives

Morpholine or piperidine (1 mmol), β -naphthol (1 mmol), sugar (1 mmol), and a catalytic amount of Sm_2O_3 NPs (5 mol%) were mixed and reacted in ethanol (10 ml) under reflux conditions. The progress of the reaction was monitored by TLC using n-hexane: ethyl acetate (1:1) and detected by a UV lamp (254 & 366 nm). At the end of the reaction, the catalyst was separated by centrifugation, filtered, washed with ethanol and water, dried at 80°C for 1h, and reused for the same reaction. The residue of the reaction mixture was evaporated, and the crude product was purified by recrystallization using ethanol and water. The products were determined by CHN analyses, NMR, and FT-IR spectra. The synthetic route for the same has been presented in Scheme 1.

2.4. (2R,3R,4R,5S)-6-(2-hydroxynaphthalen-1-yl)-6-morpholinohexane-1,2,3,4,5-pentaol (1)

Reaction of Morpholine (1 mmol), β -naphthol (1 mmol), and d-glucose (1 mmol), yellow powder. FT-IR spectrum, ν, cm^{-1} : 3418.82 (OH), 3015.33 (CH_{Ar}), 2921.75 ($\text{CH}_{\text{Aliphatic}}$), 2857.66 ($\text{CH}_{\text{Aliphatic}}$), 1628.14 (C=C), 1600 (C=C), 1514.55, 1456.46 (C=C), 1394 (C-N), 1274.14 (C-N),



Scheme 1- Synthesis of compound 4.

1113.14 (C-O), 1020.00 (C-O). ¹H NMR spectrum (400 MHz, DMSO-d₆), δ ppm (J, Hz): 8.52 (s, 1H, OH), 7.71 (dd, 2H, J = 2.4, 7.7 Hz, CH_{Ar}), 7.63 (d, 1H, J = 8.0 Hz, CH_{Ar}), 7.34 (t, 1H, J = 7.3 Hz, CH_{Ar}), 7.21 (t, 1H, J = 7.2 Hz, CH_{Ar}), 7.17 (d, 1H, J = 2.4 Hz, CH_{Ar}), 4.02-4.98 (br, 5H, OH), 3.55-3.74 (br, 7H, CH, CH₂), 3.52 (t, 2H, J = 4.8 Hz, CH_{morpho}), 3.48 (t, 2H, J = 5.2 Hz, CH_{morpho}), 3.39 (t, 2H, J = 4.8 Hz, CH_{morpho}), 3.37 (t, 2H, J = 5.2 Hz, CH_{morpho}). ¹³C NMR spectrum (100 MHz, DMSO-d₆), δ, ppm: 161.65, 156.04, 135.09, 129.66, 128.04, 127.96, 126.52, 126.37, 122.98, 119.28, 109.15, 78.73, 78.07, 70.76, 69.24, 67.14, 66.16, 47.69, 45.60. Found, %: C, 60.85; H, 6.77; N, 3.45. C₂₀H₂₇NO₇ (393.18). Calculated, %: C, 61.06; H, 6.92; N, 3.56.

2.5. (2R,3S,4R,5S)-6-(2-hydroxynaphthalen-1-yl)-6-morpholinohexane-1,2,3,4,5-pentaol (2)

Reaction of Morpholine (1 mmol), β-naphthol (1 mmol), and d-galactose (1 mmol), yellow powder. FT-IR spectrum, ν, cm⁻¹: 3417.72 (OH), 3013.52 (CH_{Ar}), 2922.30 (CH_{Aliphatic}), 2855.56 (CH_{Aliphatic}), 1599.20 (C=C), 1513.87 (C=C), 1445.88 (C=C), 1391.90 (C-N), 1271.38 (C-N), 1111.81 (C-O), 1020.00 (C-O). ¹H NMR spectrum (400 MHz, DMSO-d₆), δ ppm (J, Hz): 8.48 (s, 1H, OH), 7.73 (t, 1H, J = 7.6 Hz, CH_{Ar}), 7.64 (d, 1H, J = 8.4 Hz, CH_{Ar}), 7.35 (t, 1H, J = 7.2 Hz, CH_{Ar}), 7.22 (t, 1H, J = 8.0 Hz, CH_{Ar}), 7.12 (t, 1H, J = 2.0 Hz, CH_{Ar}), 7.10 (d, 1H, J = 2.4 Hz, CH_{Ar}), 4.02-5.00 (br, 5H, OH), 3.64-3.80 (br, 5H, CH, CH₂), 3.62 (d, 1H, J = 7.0 Hz, CH_{galactose}), 3.56 (t, 2H, J = 4.8 Hz, CH_{morpho}), 3.51 (t, 2H, J = 5.2 Hz, CH_{morpho}), 3.45 (d, 1H, J = 6.8 Hz, CH_{galactose}), 3.38 (t, 2H, J = 5.2 Hz, CH_{morpho}), 3.36 (t, 2H, J = 4.4 Hz, CH_{morpho}). ¹³C NMR spectrum (100 MHz, DMSO-d₆), δ, ppm: 161.51, 156.29, 135.13, 129.58, 127.99, 127.96, 126.45, 126.35, 122.84, 119.38, 109.10, 72.48, 71.29, 71.15, 67.18, 66.19, 63.43, 45.56. Found, %: C, 61.34; H, 7.03; N, 3.52. C₂₀H₂₇NO₇ (393.18). Calculated, %: C, 61.06; H, 6.92; N, 3.56. 61.34 (61.06); 7.03 (6.92); 3.52 (3.56).

2.6. (2R,3S,4S)-5-(2-hydroxynaphthalen-1-yl)-5-morpholinopentane-1,2,3,4-tetraol (3)

Reaction of Morpholine (1 mmol), β-naphthol (1 mmol), and d-ribose (1 mmol), yellow powder. FT-IR spectrum, ν, cm⁻¹: 3426.61 (OH), 3052.11 (CH_{Ar}), 2927.51 (CH_{Aliph}), 2885.13 (CH_{Aliph}), 1600.31 (C=C), 1402.87 (C=C), 1108.82 (C-O), 1072.86 (C-O). ¹H NMR spectrum (400 MHz, DMSO-d₆), δ ppm (J, Hz): 8.48 (s, 1H, OH), 7.73 (t, 1H, J = 6.8, CH_{Ar}), 7.64 (d, 1H, J = 8.4 Hz, CH_{Ar}), 7.60 (d, 1H, J =

7.2 Hz, CH_{Ar}), 7.48 (d, 1H, J = 8.4 Hz, CH_{Ar}), 7.44 (t, 1H, J = 7.2 Hz, CH_{Ar}), 7.36 (t, 1H, J = 7.6 Hz, CH_{Ar}), 7.22 (t, 1H, J = 7.6 Hz, CH_{Ar}), 7.07 (t, 2H, J = 2.4 Hz, CH_{Ar}), 7.03 (d, 1H, J = 7.6 Hz, CH_{Ar}), 3.34-4.21 (br, 15H, CH OH). ¹³C NMR spectrum (100 MHz, DMSO-d₆), δ, ppm: 177.31, 167.39, 161.53, 156.12, 141.33, 135.10, 134.43, 130.40, 129.63, 129.50, 128.56, 128.44, 128.03, 127.96, 126.49, 126.36, 122.92, 122.77, 119.36, 119.28, 74.15, 70.59, 63.75, 56.50, 45.57. C₁₉H₂₅NO₆ (363.17). Calculated, %: C, 62.80; H, 6.93; N, 3.85.

2.7. (2R,3S,4R)-5-(2-hydroxynaphthalen-1-yl)-5-morpholinopentane-1,2,3,4-tetraol (4)

Reaction of Morpholine (1 mmol), β-naphthol (1 mmol), and d-arabinose (1 mmol), yellow powder. FT-IR spectrum, ν, cm⁻¹: 3411.94 (OH), 3043.74 (CH_{Ar}), 2920.57 (CH_{Aliph}), 2855.01 (CH_{Aliph}), 1600.82 (C=C), 1514.72 (C=C), 1448.79 (C=C), 1393.62 (C-N), 1070.62 (C-O), 1010.37 (C-O). ¹H NMR spectrum (400 MHz, DMSO-d₆), δ ppm (J, Hz): 8.01 (s, 1H, OH), 7.73 (dd, 2H, J = 2.8, 8.0 Hz, CH_{Ar}), 7.64 (d, 1H, J = 8.4 Hz, CH_{Ar}), 7.36 (dt, 1H, J = 1.2, 7.6 Hz, CH_{Ar}), 7.22 (dt, 1H, J = 1.2, 7.2 Hz, CH_{Ar}), 7.16 (d, 1H, J = 2.4 Hz, CH_{Ar}), 7.13 (dd, 1H, J = 2.4, 8.8 Hz, CH_{Ar}), 3.66 (br, 2H, CH), 3.54 (t, 4H, J = 4.8 Hz, CH₂), 3.50 (t, 4H, J = 5.2 Hz, CH₂), 3.38 (t, 2H, J = 5.6 Hz, CH), 3.33 (t, 2H, J = 4.8 Hz, CH), 2.90 (br, 2H, CH₂), 4.01-5.40 (br, 4H, OH). ¹³C NMR spectrum (100 MHz, DMSO-d₆), δ, ppm: 161.50, 155.99, 152.60, 135.10, 129.68, 128.12, 127.98, 126.51, 126.39, 122.99, 119.22, 74.18, 71.17, 67.16, 67.01, 44.57, 44.17. Found, %: C, 62.87; H, 6.97; N, 3.87. C₁₉H₂₅NO₆ (363.17). Calculated, %: C, 62.80; H, 6.93; N, 3.82.

2.8. (2R,3R,4R,5S)-6-(2-hydroxynaphthalen-1-yl)-6-(piperidin-1-yl)hexane-1,2,3,4,5-pentaol (5)

Reaction of piperidine (1 mmol), β-naphthol (1 mmol), and d-glucose (1 mmol), yellow powder. FT-IR spectrum, ν, cm⁻¹: 3401.85 (OH), 3057.27 (NH), 2935.50 (CH_{Ar}), 2856.07 (CH_{Aliph}), 1627.46 (C=C), 1588.26 (C=C), 1512.98 (C=C), 1373.25 (C-N), 1271.89 (C-N), 1119.08 (C-O), 1081.38 (C-O). ¹H NMR spectrum (400 MHz, DMSO-d₆), δ ppm (J, Hz): 7.94 (s, 1H, OH), 7.75 (d, 1H, J = 2.8 Hz, CH_{Ar}), 7.73 (d, 1H, J = 3.6 Hz, CH_{Ar}), 7.67 (d, 1H, J = 8.4 Hz, CH_{Ar}), 7.37 (dt, 1H, J = 1.2, 6.8 Hz, CH_{Ar}), 7.24 (dt, 1H, J = 1.2, 7.6 Hz, CH_{Ar}), 7.15 (d, 1H, J = 2.0 Hz, CH_{Ar}), 7.11 (dd, 1H, J = 2.4, 8.8 Hz, CH_{Ar}), 3.31 (t, 1H, J = 5.6 Hz, CH), 3.24 (t, 1H, J = 5.2 Hz, CH), 2.92 (br, 2H, CH₂), 1.56 (br, 5H, CH,

CH₂), 1.48 (br, 2H, CH), 1.40 (m, 2H, CH), 1.37 (m, 3H, CH, CH₂). ¹³C NMR spectrum (100 MHz, DMSO-d₆), δ, ppm: 161.05, 155.86, 135.08, 129.72, 128.16, 127.99, 126.53, 126.42, 123.04, 119.13, 109.13, 109.11, 88.44, 48.48, 46.21, 44.13, 26.65, 25.61, 25.32, 24.64, 24.07, 22.84, 22.36. Found, %: C, 64.96; H, 7.11; N, 3.47. C₂₁H₂₉NO₆ (391.46). Calculated, %: C, 64.43; H, 7.47; N, 3.58.

2.9. (2R,3S,4R,5S)-6-(2-hydroxynaphthalen-1-yl)-6-(piperidin-1-yl)hexane-1,2,3,4,5-pentaol (6)

Reaction of piperidine (1 mmol), β-naphthol (1 mmol), and d-galactose (1 mmol), yellow powder. FT-IR spectrum, ν, cm⁻¹: 3429.45 (OH), 3057.19 (CH_{Ar}), 2932.97 (CH_{Aliph}), 1625.51 (C=C), 1513.58 (C=C), 1447.80 (C=C), 1373.90 (C-N), 1243.45 (C-O), 1214.23 (C-O), 1001.22 (C-O). ¹H NMR spectrum (400 MHz, DMSO-d₆), δ ppm (J, Hz): 7.95 (s, 1H, OH), 7.89 (d, 1H, J = 8.0 Hz, CH_{Ar}), 7.71-7.76 (m, 1H, CH_{Ar}), 7.66 (d, 1H, J = 8.4 Hz, CH_{Ar}), 7.61 (d, 1H, J = 8.8 Hz, CH_{Ar}), 7.37 (t, 1H, J = 7.6 Hz, CH_{Ar}), 7.25 (m, 1H, CH_{Ar}), 7.09 (d, 1H, J = 7.6 Hz, CH_{Ar}), 7.07 (m, 1H, CH_{Ar}), 3.34 (q, 2H, J = 6.8 Hz, CH), 3.32 (t, 2H, J = 5.6 Hz, CH), 3.27 (t, 2H, J = 5.6 Hz, CH), 3.23 (br, 1H, CH), 3.18 (s, 1H, CH), 3.15 (br, 2H, CH, CH₂), 2.92 (br, 2H, CH), 1.57 (d, 4H, J = 5.2 Hz, CH₂), 1.46 (t, 3H, J = 5.6 Hz, CH, CH₂), 1.34-1.40 (b, 5H, CH, CH₂), 1.21 (br, 1H, CH), 1.06 (t, 1H, J = 6.8, CH). ¹³C NMR spectrum (100 MHz, DMSO-d₆), δ, ppm: 161.05, 157.02, 155.78, 146.15, 135.06, 131.14, 129.91, 129.73, 128.44, 128.16, 127.50, 126.54, 125.64, 125.55, 124.66, 123.05, 122.53, 121.82, 119.08, 111.84, 109.09, 88.44, 48.48, 46.20, 44.15, 26.66, 25.61, 25.33, 24.64, 24.08, 22.85, 22.32. Found, %: C, 64.57; H, 7.73; N, 3.62. C₂₁H₂₉NO₆ (391.46). Calculated, %: C, 64.43; H, 7.47; N, 3.58.

3. Results and discussion

The present paper reports the results of research aimed at the synthesis of some nitrogen heterocyclic compounds like morpholine and piperidine using biosynthesized Sm₂O₃ NPs from purple Rose of Sharon flower extract.

Some parameters like phytochemicals, phytochemical concentration, metal salt concentration, pH, and temperature can control the morphology, yield, stability, and rate of nanoparticle formation. The phytochemicals present in plant extracts of the reaction mixture have the potential to oxidize the metal ions in a much shorter time as compared to other methods. Therefore, extracts

are considered to be an excellent source for metal and metal oxide nanoparticle synthesis. GC-Mass analyses of the Rose of Sharon flower were performed and various bioactive compounds like 1-decyne, 2,3-dihydro-3,5-dihydroxy-6-methyl-4H-pyran-4-one, cytidine, gamma sitosterol, stigmasterol, aristolone, alpha amyirin, bis(2-ethylhexyl) phthalate, eicosane, ethyl linoleate, elcosa methyl cyclodeca siloxane, hexadecanoic acid, 2-hydroxy-1-(hydroxymethyl)ethyl ester, and octadecanal were identified.

The effects of the reaction conditions such as the ratio of plant extract and Sm(NO₃)₃, pH, reaction time, and reaction temperature were studied to maximize the yield of the nano compounds. The resulting solutions of the reaction were monitored using a UV-Vis spectrophotometer. The optimized condition of the reaction was obtained at room temperature in pH=10 after 24 h with the ratio of 1:1 of plant extract and samarium nitrate solution.

Completion of the reaction between Rose of Sharon flower extract, and samarium nitrate Sm(NO₃)₃ was monitored and optimized by taking the absorption spectrum in UV-Vis spectrophotometer at different reaction conditions. As the Rose of Sharon flower extract was added to the aqueous samarium nitrate solution, the color of the solution changed to colloidal dark brown with Sm₂O₃ colloids formation. The UV-Vis spectra were recorded after 10 min, 20 min, 60 min, 16 h, and 24 h at different temperatures (25°C, 45°C, 60°C, and 90°C) from the initiation of reaction at the wavelength of 200-800 nm. Absorption UV-Vis spectra of biosynthesized Sm₂O₃ hybrid showed λ maxes at 244 and 324 nm (Fig. 1). The absorption peaks found between 300 and 500 nm were assigned to the corresponding peaks. The broad

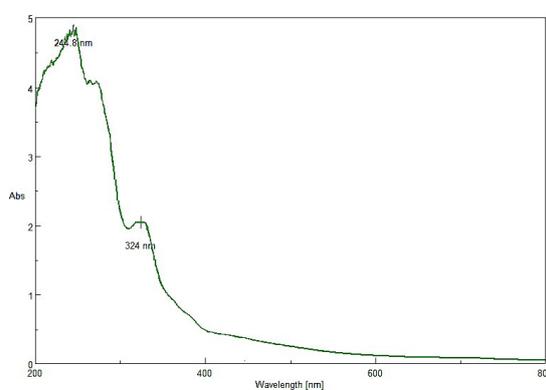


Fig. 1- UV-Vis spectrum of biosynthesized Sm₂O₃ after 24h with the ratio of Sm(NO₃)₃: Rose of Sharon flower extract (1:1).

absorption below 300 nm was possibly due to the O^{2-} - Sm^{3+} charge transfer [31,32]. It is well known from absorption spectroscopy that the bandgap increases on decreasing particle size. There is also an opposite ratio between bandgap and the wavelength of absorption. The absorption bands of the synthesized Sm_2O_3 nanocomposite have shown a blue shift. This optical phenomenon indicates that these nanoparticles show the quantum size effect and can be due to a high decrease in particle size [33, 34]. The possible interaction between $Sm(NO_3)_3 \cdot 6H_2O$ and Rose of Sharon flower extract was investigated using FT-IR spectroscopy, which leads to the preparation and stabilization of Sm_2O_3 NPs. The results of FT-IR spectra show that the data are the same as reported in the literature [35]. The broad strong absorption bands belonging to O-Sm- and OH was shown at 600–900 and 3446 cm^{-1} , respectively. They confirmed the formation of the Sm_2O_3 NPs. The broad band at 3446 cm^{-1} is

attributed to the stretching vibration of $-OH$ and $H-O-H$ molecules absorbed physically on the surface of Sm_2O_3 NPs.

The crystalline structure and average size of nanoparticles of Sm_2O_3 were identified with the XRD technique. As shown in Fig. 2, the XRD pattern of Sm_2O_3 nanoparticles shows high intense peaks in the whole spectrum of 2θ values ranging from 20° to 80° , which correspond to the hexagonal phase of Sm_2O_3 nanoparticles. They are consistent with the standard pattern for JCPDS Card No. (98-002-3666 and 98-006-2022) [38, 39] and confirmed that Sm_2O_3 nanoparticles had been formed. The average diameter is obtained as about 35.6 nm according to the line width analysis of the diffraction peaks based on the Debye-Scherrer equation [40] ($D=K\lambda/\beta\cos\theta$, where K is constant, β is the peak width at half maximum and λ is X-ray wavelength).

The SEM images in Fig. 3 show the morphology

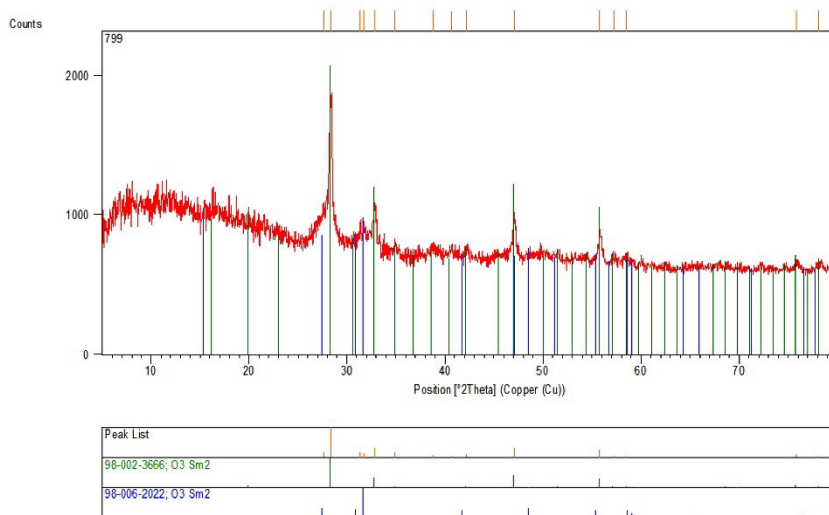


Fig. 2- XRD patterns of Sm_2O_3 NPs.

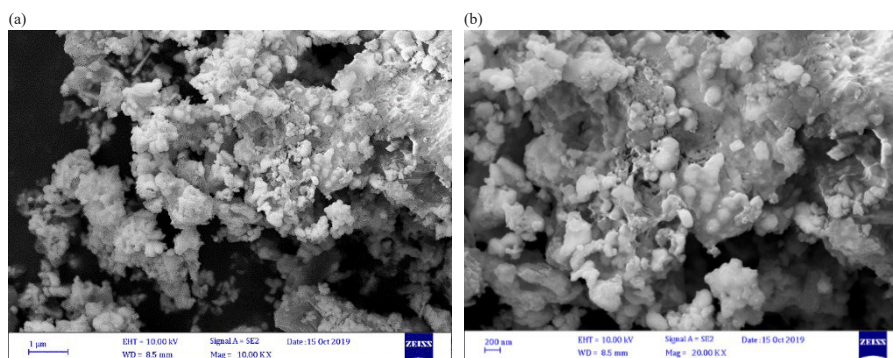


Fig. 3- SEM image of Sm_2O_3 NPs.

and particle size of Sm_2O_3 . In this method, the samples were turned to hexagonal particles with much less agglomeration when calcined at high temperatures. The particles' diameter and size were measured. Most NPs are in the range of nanometers (around 30-70 nm).

Fig. 4 shows the transmission electron microscopy (TEM) images of the Sm_2O_3 NPs. We can see that the Sm_2O_3 NPs are composed of small particles. The average particle size is about 30-70 nm.

In Fig. 5, EDX analysis was performed to confirm the elements presented in the resulting Sm_2O_3 NPs. For using SEM/EDS to analyze the composition of a sample, usually, heavy metal like Au (Au-Pd) was coated with the sample to make it conductive before inserting it into FE-SEM. So there is a sign of coating metal (Au) in EDX. Also the analysis reveals the presence of Sm and O (Sm_2O_3 NPs) in the sample.

In the preliminary stage of the investigation, the model reaction of β -naphthol, piperidine, and arabinose was carried out by using various

amounts of NPs in various solvents and solvent-free conditions. The optimum amount of Sm_2O_3 NPs was 5 mol% as shown in Table 1. Increasing the amount of catalysts by more than 5 mol% does not improve the yield of the product any further, whereas decreasing the amount of catalyst leads to a decrease in the product (Table 1).

It was found that in the absence of Sm_2O_3 NPs, the yield of the product on the TLC plate even after 3h of the reaction was not good. The best results were obtained with 5 mol% of Sm_2O_3 NPs in ethanol under reflux conditions (Table 1, Entry 14).

To evaluate the scope and limitations of this methodology, we extended our studies to include a variety of structurally different sugars with β -naphthol, morpholine, or piperidine. The results are summarized in Table 2 (entries 1-6). In almost all cases, the reactions proceeded smoothly within 60-90 min, providing the corresponding products in good isolated yields.

The structures of compounds 1-6 are confirmed

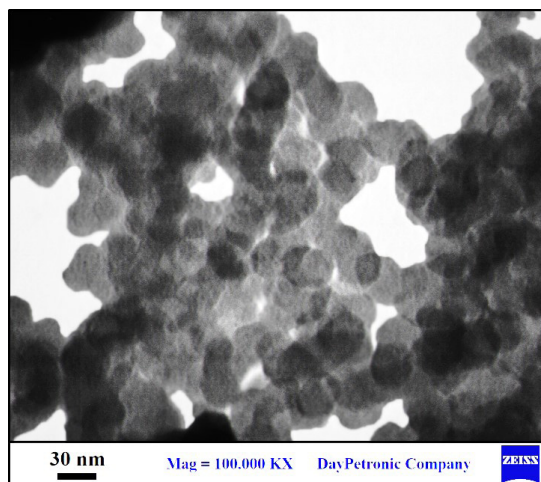


Fig. 4- TEM image of Sm_2O_3 NPs.

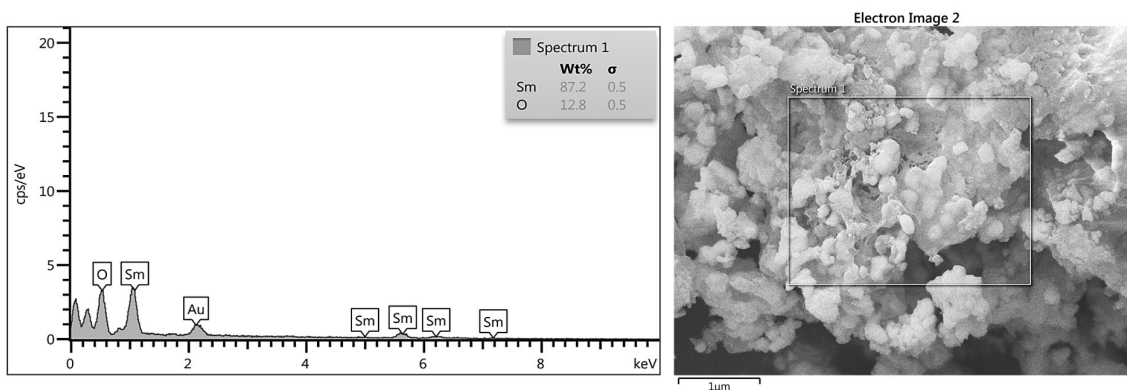


Fig. 5- Energy dispersive spectra (EDS) of Sm_2O_3 NPs.

Table 1- The reaction of β -naphthol (1 mmol), piperidine (1 mmol) and arabinose (1 mmol) under different conditions

Entry	Solvent	Sm ₂ O ₃ NPs (mol%) as a catalyst	Time (hours)	Yield ^a (%)
1	THF	-	3	trace
2	THF	3	3	32
3	THF	4	1	56
4	THF	5	1	82
5	THF	7	1	84
6	H ₂ O	-	1	trace
7	H ₂ O	3	3	24
8	H ₂ O	4	1	37
9	H ₂ O	5	1	58
10	H ₂ O	7	1	56
11	EtOH	-	3	trace
12	EtOH	3	3	45
13	EtOH	4	1	72
14	EtOH	5	1	96
15	EtOH	7	1	96
16	CH ₂ Cl ₂	-	3	-
17	CH ₂ Cl ₂	3	3	33
18	CH ₂ Cl ₂	4	2	46
19	CH ₂ Cl ₂	5	2	76
20	CH ₂ Cl ₂	7	2	78
21	Solvent-free	-	4	trace
22	Solvent-free	3	4	58
23	Solvent-free	4	2	62
24	Solvent-free	5	2	76
25	Solvent-free	7	2	77

^a Isolate Yield.

by IR, ¹H NMR, ¹³C NMR, and CHN analysis. For example, the ¹H NMR spectrum of compound 4 shows singlet at 8.01 ppm for OH proton of β -naphthol and signals at 4.01-5.40 ppm for OH protons. The aromatic protons were presented at 7.13-7.73 ppm. In the ¹³C NMR spectrum, the resonances related to carbon groups of HO-C- were appeared at 67.16, 67.01, 44.57, and 44.17 ppm. The signals attributed to unsaturated carbon double bonds (-CH=CH-) have appeared at 155.99, 152.60, 135.10, 129.68, 128.12, 127.98, 126.51, 126.39, 122.99, and 119.22 ppm, respectively. FT-IR spectra of compounds (1-6) have been investigated in the frequency range 400–4000 cm⁻¹. The bands at about 1602-1624 and 1438-1542 cm⁻¹ belonged to the C=C double bonds stretching vibration of the synthesized compounds. The bands at about 1017-1402 cm⁻¹ indicated the existence of C-O and C-N groups. The elemental analysis result of compound 4 was satisfactory.

A plausible mechanism [39] for the reaction is envisaged in (Scheme 2). It is proposed that the carbonyl group of aldehyde (sugars) primarily is activated by NPs (Sm³⁺) followed by an intermediate formation. The carbonyl group of this resulting

intermediate is activated again with Sm³⁺ further reacts with the HN group of amine to obtain compound 4 as shown in Scheme 2.

To investigate the efficiency of the Sm₂O₃ NPs, we compared some other metal oxide NPs for the synthesis of compound 4 and the results were summarized in Table 3. The metal oxide NPs were synthesized according to the previously reported procedures [40-45]. As shown in Table 3, the best catalyst for the synthesis of compound 4 is Sm₂O₃ NPs, using this metal oxide as a catalyst offers several advantages such as excellent yields, short reaction times, a simple procedure, and using EtOH as a green solvent in contrast with other metal oxides. Sm₂O₃ NPs as an efficient heterogeneous catalyst were prepared by a simple operation from Rose of Sharon flower extract.

The catalyst was easily recovered by centrifugation, washed with ethanol, and dried at 80 °C for 2 h. The recovered catalyst was then added to a fresh reaction mixture under the same conditions and reused 4 times without significant loss of activity (Table 4). Further recycling of the nanocatalyst led to a gradual loss of the catalyst during the recovering and washing stages.

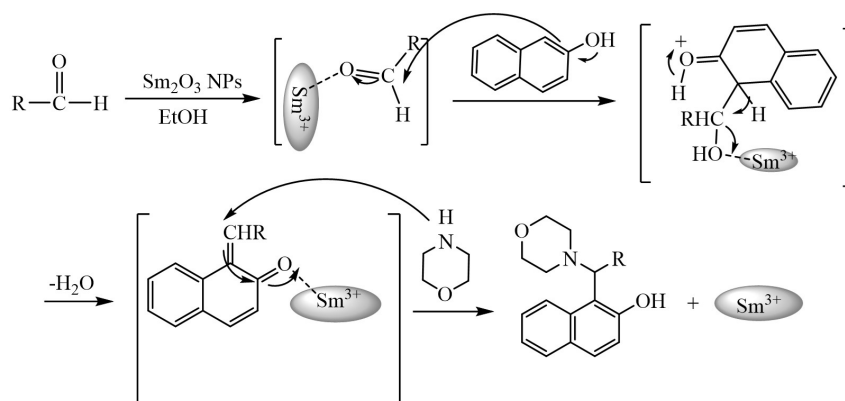
Scheme 2- A plausible mechanism for synthesis of compound 4 using Sm_2O_3 NPs.

Table 3- A comparison of different catalysts for the synthesis of compound 5 in EtOH

Entry	Catalyst	Amount of catalyst (mol%)	Time (hours)	Yield %
1	CuO	10	4	48
2	Fe_3O_4 MNPs	10	4	64
3	$\text{Fe}_3\text{O}_4@/\text{SiO}_2\text{-SO}_3\text{H}$ MNPs	7	3	78
4	CaO NPs	7	4	46
5	ZnO-CaO NPs	7	3	83
6	Sm_2O_3 Bulk	7	4	49
7	Sm_2O_3 NPs	5	2	96

Table 4- Recycling of the Sm_2O_3 NPs catalyst

Number of cycles	Yield ^a (%)
1	96
2	96
3	95
4	94

^a Isolated yield after chromatography

4. Conclusions

In summary, an efficient protocol for the synthesis of morpholine and piperidine derivatives was described with the reaction of β -naphthol, morpholine, or piperidine, and monosaccharide using Sm_2O_3 NPs as a reusable catalyst in ethanol. The reactions were carried out in short reaction times and the corresponding products were obtained in good yields. In addition to having the general advantages attributed to the inherent property of nanocatalyst, Sm_2O_3 NPs exhibited exceptionally high catalytic activity in green chemistry and increases reaction speed without pollution.

Acknowledgment

The authors wish to thank the University of Guilan and the Islamic Azad University of Qaemshahr Branch for their institutional support.

References

- Pan T, He X, Chen B, Chen H, Geng G, Luo H, et al. Development of benzimidazole derivatives to inhibit HIV-1 replication through protecting APOBEC3G protein. *European Journal of Medicinal Chemistry*. 2015;95:500-13.
- Zhao Ja, Guo Y, Hu J, Yu H, Zhi S, Zhang J. Potential anticancer activity of benzimidazole-based mono/dinuclear Zn(II) complexes towards human carcinoma cells. *Polyhedron*. 2015;102:163-72.
- Salahuddin, Shaharyar M, Mazumder A. Benzimidazoles: A biologically active compounds. *Arabian Journal of Chemistry*. 2017;10:S157-S73.
- Achar KCS, Hosamani KM, Seetharamareddy HR. In-vivo analgesic and anti-inflammatory activities of newly synthesized benzimidazole derivatives. *European Journal of Medicinal Chemistry*. 2010;45(5):2048-54.
- Mahmood K, Hashmi W, Ismail H, Mirza B, Twamley B, Akhter Z, et al. Synthesis, DNA binding and antibacterial activity of metal(II) complexes of a benzimidazole Schiff base. *Polyhedron*. 2019;157:326-34.
- Bektas H, Albay C, Sökmen BB, Aydın S, Menteşe E, Aydın G, et al. Synthesis, Antioxidant, and Antibacterial Activities of Some New 2-(3-fluorobenzyl)-1 H-benzimidazole Derivatives. *Journal of Heterocyclic Chemistry*. 2018;55(10):2400-7.

7. Trivedi R, De SK, Gibbs RA. A convenient one-pot synthesis of 2-substituted benzimidazoles. *Journal of Molecular Catalysis A: Chemical*. 2006;245(1-2):8-11.
8. Bai Y, Lu J, Shi Z, Yang B. Synthesis of 2,15-hexadecanedione as a precursor of Muscone. *Synlett*. 2001;2001(04):0544-6.
9. Hasegawa E, Yoneoka A, Suzuki K, Kato T, Kitazume T, Yanagi K. Reductive transformation of α,β -epoxy ketones and other compounds promoted through photoinduced electron transfer processes with 1,3-dimethyl-2-phenylbenzimidazoline (DMPBI). *Tetrahedron*. 1999;55(45):12957-68.
10. Harkala KJ, Eppakayala L, Maringanti TC. Synthesis and biological evaluation of benzimidazole-linked 1,2,3-triazole congeners as agents. *Org Med Chem Lett*. 2014;4(1):14-.
11. Heravi MM, Nami N, Oskooie HA, Hekmatshoar R. Synthesis of Thiazinobenzimidazole Derivatives in a Solventless System Under Microwave Irradiation. *Phosphorus, Sulfur, and Silicon and the Related Elements*. 2005;180(7):1605-10.
12. Vahedi H, Nami N, Nami N. Synthesis and Structure Elucidation of 4-(4-Amino-5-thioxo-4,5-dihydro-1H-1,2,4-triazol-3-yl-methylene)-2-phenyl-1 H-imidazol-5 (4H)-one. *E-Journal of Chemistry*. 2010;7(3):1116-9.
13. Nami N, Hosseinzadeh M, Nami N, Haghdadi M. Synthesis of Substituted Pyrazino[5,6-b]pyrimidine and Some Indole Derivatives. *Phosphorus, Sulfur, and Silicon and the Related Elements*. 2009;184(11):2846-55.
14. Penieres-Carrillo JG, Rios-Guerra H, Pérez-Flores J, Rodríguez-Molina B, Torres-Reyes Á, Barrera-Téllez F, et al. Reevaluating the synthesis of 2,5-disubstituted-1 H -benzimidazole derivatives by different green activation techniques and their biological activity as antifungal and antimicrobial inhibitor. *Journal of Heterocyclic Chemistry*. 2019;57(1):436-55.
15. Kaveh S, Nami N, Norouzi B, Mirabi A. Biosynthesis of (MWCNTs)-COOH/CdO hybrid as an effective catalyst in the synthesis of pyrimidine-thione derivatives by water lily flower extract. *Inorganic and Nano-Metal Chemistry*. 2021;51:1459-1470.
16. Bouzigues C, Gacoin T, Alexandrou A. Biological Applications of Rare-Earth Based Nanoparticles. *ACS Nano*. 2011;5(11):8488-505.
17. Singh S, Srivastava P, Kapoor IPS, Singh G. Preparation, characterization, and catalytic activity of rare earth metal oxide nanoparticles. *Journal of Thermal Analysis and Calorimetry*. 2012;111(2):1073-82.
18. Ullah N, Song Z, Liu W, Kuo C-C, Ramiere A, Cai X. Photo-promoted in situ reduction and stabilization of Pd nanoparticles by H₂ at photo-insensitive Sm₂O₃ nanorods. *Journal of Colloid and Interface Science*. 2022;607:479-87.
19. Abdoli M, Nami N, Hossaini Z. One-pot synthesis of spiro-acridine/indoline and indoline derivatives using (MWCNTs)-COOH/La₂O₃ hybrid as an effective catalyst. *Journal of Heterocyclic Chemistry*. 2020;58(2):523-33.
20. Song H-W, Kim N-Y, Park J-e, Ko J-H, Hickey RJ, Kim Y-H, et al. Shape-controlled syntheses of metal oxide nanoparticles by the introduction of rare-earth metals. *Nanoscale*. 2017;9(8):2732-8.
21. Kovalchukova OV, Bostanabad AS, Lobanov NN, Rudakova TA, Strashnov PV, Skarzhenskii YA, et al. Copper(II) alkyl- and benzylnitrosohy-droxylamines as precursors for the synthesis of copper(i) oxide micro- and nanoparticles of various morphologies. *Inorganic Materials*. 2014;50(11):1093-8.
22. Zhu W, Xu L, Ma J, Yang R, Chen Y. Effect of the thermodynamic properties of W/O microemulsions on samarium oxide nanoparticle size. *Journal of Colloid and Interface Science*. 2009;340(1):119-25.
23. Qiu J-D, Zhou W-M, Guo J, Wang R, Liang R-P. Amperometric sensor based on ferrocene-modified multiwalled carbon nanotube nanocomposites as electron mediator for the determination of glucose. *Analytical Biochemistry*. 2009;385(2):264-9.
24. Sone BT, Manikandan E, Gurib-Fakim A, Maaza M. Sm₂O₃ nanoparticles green synthesis via *Callistemon viminalis*' extract. *Journal of Alloys and Compounds*. 2015;650:357-62.
25. Gao J, Zhao Y, Yang W, Tian J, Guan F, Ma Y, et al. Preparation of samarium oxide nanoparticles and its catalytic activity on the esterification. *Materials Chemistry and Physics*. 2003;77(1):65-9.
26. Chin WC, Cheong KY, Hassan Z. Sm₂O₃ gate dielectric on Si substrate. *Materials Science in Semiconductor Processing*. 2010;13(5-6):303-14.
27. Michel CR, Martínez-Preciado AH, Parra R, Aldao CM, Ponce MA. Novel CO₂ and CO gas sensor based on nanostructured Sm₂O₃ hollow microspheres. *Sensors and Actuators B: Chemical*. 2014;202:1220-8.
28. Heidarzadeh T, Nami N, Zareyee D. Preparation of (MWCNTs)-COOH/CeO₂ hybrid as an efficient catalyst for Claisen-Schmidt condensation. *Journal of Applied Chemical Research*. 2021;15:44-57.
29. Kaveh S, Norouzi B, Nami N, Mirabi A. Phytochemical synthesis of CdO nanoparticles: fabrication of electrochemical sensor for quantification of cefixime. *Journal of Materials Science: Materials in Electronics*. 2021;32(7):8932-43.
30. Nami N, Neumuller B, Heravi MM, Haghdadi M. Synthesis and crystal structure of chiral hydroquinoxaline derivatives. *Mendeleev Communications*. 2008;18(3):153-5.
31. Zhang H, Dai H, Liu Y, Deng J, Zhang L, Ji K. Surfactant-mediated PMMA-templating fabrication and characterization of three-dimensionally ordered macroporous Eu₂O₃ and Sm₂O₃ with mesoporous walls. *Materials Chemistry and Physics*. 2011;129(1-2):586-93.
32. Kang J-G, Min B-K, Sohn Y. Synthesis and characterization of Sm(OH)₃ and Sm₂O₃ nanoroll sticks. *Journal of Materials Science*. 2014;50(4):1958-64.
33. Ye XR, Daraio C, Wang C, Talbot JB, Jin S. Room Temperature Solvent-Free Synthesis of Monodisperse Magnetite Nanocrystals. *Journal of Nanoscience and Nanotechnology*. 2006;6(3):852-6.
34. Guo-hua Z, Ming-fang L, Ming-li L. Differential pulse voltammetric determination of dopamine with the coexistence of ascorbic acid on boron-doped diamond surface. *Open Chemistry*. 2007;5(4):1114-23.
35. Yousefi T, Mostaei MT, Ghasemi M, Ghadirifar A. A Simple Way to Synthesize of Samarium Oxide Nanoparticles: Characterization and Effect of pH on Morphology. *Synthesis and Reactivity in Inorganic, Metal-Organic, and Nano-Metal Chemistry*. 2015;46(1):137-42.
36. Wiarda D, Uhrmacher M, Lieb KP, Bartos A. Golden book of phase, Transitions. Wroclaw. 2002;1:1.
37. Jiang S, Liu J, Lin C, Li X, Li Y. High-pressure x-ray diffraction and Raman spectroscopy of phase transitions in Sm₂O₃. *Journal of Applied Physics*. 2013;113(11):113502.
38. Warren- Aver bach Applications. *Industrial Applications of X-Ray Diffraction*: CRC Press; 1999. p. 865-86.
39. Singh RK, Duvedi R. Environment-friendly green chemistry approaches for an efficient synthesis of 1-amidoalkyl-2-naphthols catalyzed by tannic acid. *Arabian Journal of Chemistry*. 2018;11(1):91-8.
40. Phiw dang K, Suphankij S, Mekprasart W, Pecharapa W. Synthesis of CuO Nanoparticles by Precipitation Method Using Different Precursors. *Energy Procedia*. 2013;34:740-5.
41. Rostami Z, Rouhanizadeh M, Nami N, Zareyee D. Fe₃O₄

magnetic nanoparticles (MNPs) as an effective catalyst for synthesis of indole derivatives. *Nanochemistry Research*. 2018;3:142-148.

42. Nami N, Nami N. Efficient solvent-free synthesis of amidines using nano-Fe₃O₄ encapsulated-silica particles bearing sulfonic acid. *Journal of Chemical Biological and Physical Sciences. Section B*. 2015;5:1195-1204.

43. Heidarzadeh T, Nami N, Zareyee D. Synthesis of Indole

Derivatives Using Biosynthesized ZnO-CaO Nanoparticles as an Efficient Catalyst. *Journal of Nano Research*. 2021;66:61-71.

44. The Synthesis of silver nanoparticles using Beetroot extract and its antibacterial and catalytic activity. *Eurasian Chemical Communications*. 2019;1(6):545.

45. Hasnidawani JN, Azlina HN, Norita H, Bonnia NN, Ratim S, Ali ES. Synthesis of ZnO Nanostructures Using Sol-Gel Method. *Procedia Chemistry*. 2016;19:211-6.